ACS ES&T Engineering

pubs.acs.org/estengg

Article

Flash Joule Heating Upgraded Li Leaching of Residues from Spent $LiFePO_4$ Cathodes for Superior Catalytic Degradation of Pollutants

Hua Shang, Wenting Yang, Zhelin He, Jiewen Luo, Fengbo Yu, Chao Jia, and Xiangdong Zhu*

Cite This: https://doi.org/10.1021/acsestengg.4c00645

Read Online

ACCESS | Metrics & More | Article Recommendations | Supporting Information

ABSTRACT: The rapid development of new energy sources has produced large quantities of battery-derived spent $LiFePO_4$ cathodes (SLICs), whose recycling has attracted growing attention in recent years. Previous SLICs recycling approaches have focused on the recovery of Li resources, neglecting the Fe-enriched residues obtained after Li recovery. Generally, Fe-enriched residues cannot be effectively converted to active Fe species using traditional methods, thereby limiting their upgrading. This study uses the emerging flash Joule heating (FJH) technology to upgrade Fe-enriched residues, and its performance was independent of Li leaching pathways. Common Li leaching protocols were initially applied to extract Li and produce residues enriched with FeC_2O_4, FeO(OH), $FePO_4$, and Fe_3O_4. Subsequently, ultrahigh temperature and electrical stripping were performed by FJH treatment, promoting Fe−O bond breakage within the various Fe phases and generating low-coordinated Fe^0 nanoparticles, as confirmed by extended X-ray absorption fine structure analysis. The unique low-coordinated Fe^0 nanoparticles present in the FJH-derived composites promoted the enhanced catalytic degradation of chloramphenicol following peroxydisulfate activation, in relation to that achieved through traditional pyrolysis-derived composites. Furthermore, the developed continuous FJH process demonstrated the potential for the large-scale recycling of Fe-enriched residues and promoted the conversion of Fe-enriched residues after Li recovery.

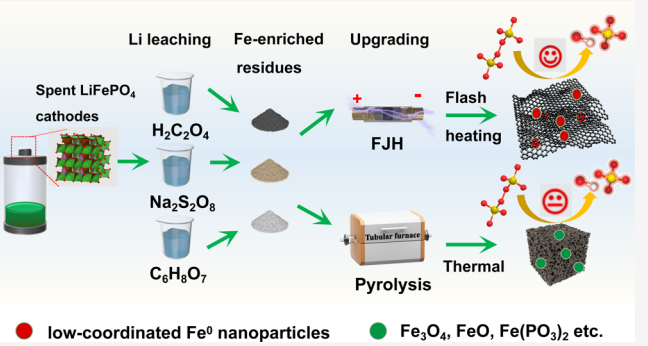

KEYWORDS: *spent lithium-ion batteries, $LiFePO_4$ cathode, recycling, flash Joule heating*

INTRODUCTION

Owing to their long cycle lives and excellent safety profiles, batteries constructed using $LiFePO_4$ cathodes have been extensively used as large-scale energy storage devices in electric vehicles.[1,2] The service lives of $LiFePO_4$ batteries tend to range from 5 to 8 years.[3] In 2021, China produced 9400 tons of spent $LiFePO_4$ batteries.[4−6] These statistics indicate the necessity to adequately dispose of a large number of spent $LiFePO_4$ cathodes (SLICs) derived from these batteries. Currently, the recycling of SLICs is mainly focused on the extraction of strategic metals such as lithium. However, the Fe-enriched residues generated from the Li leaching of SLICs have largely been ignored.[7,8] It is therefore desirable to upgrade these Fe-enriched residues to reduce resource waste and avoid possible secondary pollution by harmful residues.[9]

To date, the high-temperature upgrade of Fe-enriched residues to produce composites has attracted growing attention,[10] with pyrolysis being a particularly common approach for this process.[11] In traditional pyrolysis, its temperature may restrict the formation of active components due to the higher temperature for breaking the chemical bonds in Fe minerals,[12] thereby limiting the catalytic performance of the resulting composites.[13] In addition, graphitization levels of the carbon substrate tend to be low at such carbonization temperatures, thereby resulting in weak electron transport abilities during catalyst activation.[14] Furthermore, previous studies have indicated that the activation properties of composites derived from Fe-enriched residues tend to be dependent on the Li leaching pathway employed, such as treatment with citric acid ($C_6H_8O_7$), DL-malic acid ($C_4H_5O_6$), oxalic acid ($H_2C_2O_4$), or sodium peroxydisulfate ($Na_2S_2O_8$).[15,16] Therefore, it is necessary to develop an efficient upgrading method that can overcome these difficulties and convert Fe-enriched residues from the Li leaching of SLICs to high-quality composites.

Interestingly, flash Joule heating (FJH) has been identified as an emerging method for upgrading solid wastes.[17,18] In the FJH process, a current flows directly through the sample, which instantaneously results in the achievement of ultrahigh

Received: September 26, 2024
Revised: December 19, 2024
Accepted: December 19, 2024

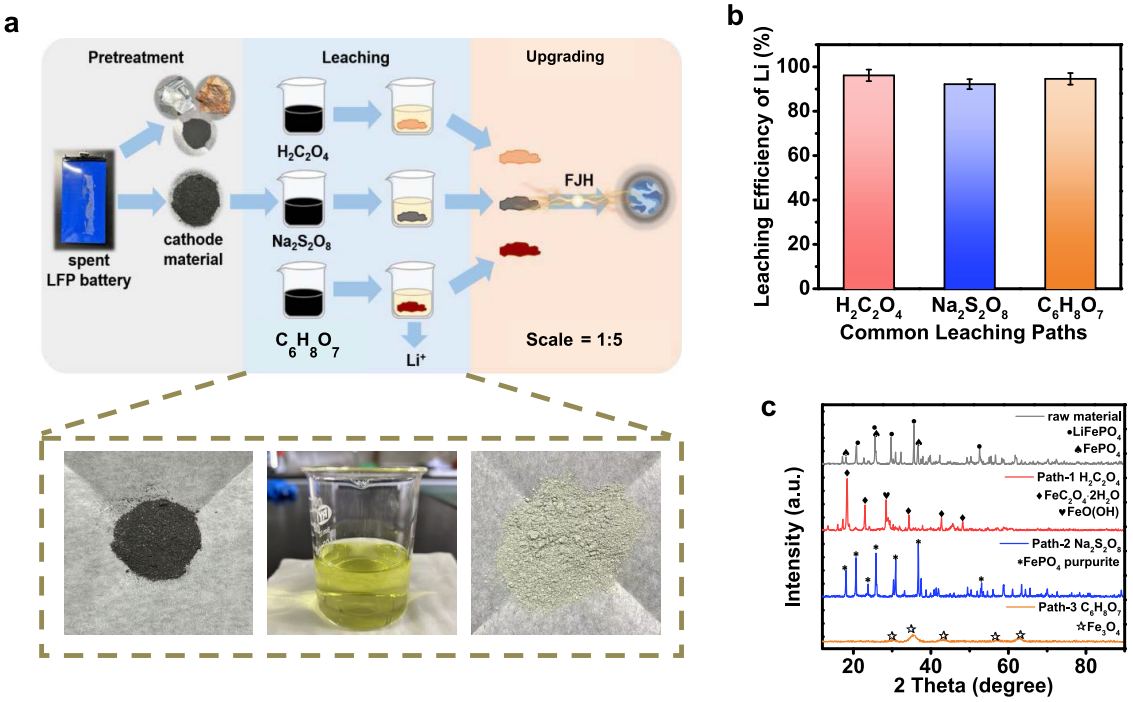

Figure 1. (a) Li leaching and synchronous obtaining Fe-enriched residues via three common leaching pathways. (b) Leaching efficiency of Li from spent LIBs cathodes within leaching solution $H_2C_2O_4$ (leaching path 1), $Na_2S_2O_8$ (leaching path 2), and $C_6H_8O_7$ (leaching path 3) [conducted at a leaching solution concentration of 0.3 mol/L, temperature of 80 °C, soild/liquid concentration of 60 g/L, and leaching time of 60 min]. (c) XRD spectra of raw materials SLICs and Fe-enriched residues after Li leaching within $H_2C_2O_4$, $Na_2S_2O_8$, and $C_6H_8O_7$ solution.

temperature, promotes electrical stripping, and induces quenching effects.[19,20] It has been found that the instantaneous ultrahigh temperature achievement and electrical stripping effect can lead to the breakage of chemical bonds such as Fe−O to form active Fe species.[21] Furthermore, these characteristics can convert the carbon substrate to a thin layer of graphene, imparting a strong electron transport ability during catalyst activation and enhancing catalyst performance.[22] As a result, the FJH method can be considered as a possible approach for upgrading Fe-enriched residues obtained from the Li leaching of SLICs.

In this study, Fe-enriched residues are initially obtained from the Li leaching of SLICs using three common leaching pathways (i.e., oxalic acid, sodium peroxydisulfate, and citric acid). The Fe-enriched residues are subsequently upgraded using the FJH treatment approach. In addition, promotion of the catalytic degradation of chloramphenicol (CAP) by the FJH-derived composites is employed as a probe to measure the performance of FJH upgrading for providing active Fe species. Moreover, the advantages of FJH treatment were evaluated from the perspective of the composite structure obtained by FJH compared with that generated via the traditional pyrolysis method. The mechanism of CAP catalytic degradation in the presence of the FJH-derived Fe composite is further discussed.

MATERIALS AND METHODS

Recovery of Li- and Fe-Enriched Residues from SLICs. Spent lithium-ion batteries (LIBs) were collected from a spent-battery recycling station in Suzhou, China. To obtain SLICs, the spent LIBs were discharged and manually disassembled. For Li recycling, three common leaching pathways (i.e., oxalic acid, sodium peroxydisulfate, and citric acid pathways) were employed to leach the SLICs, resulting in the generation of abundant Fe-enriched residues. For the oxalic acid process, a solution of oxalic acid ($H_2C_2O_4$) was used to dissolve the SLICs. Li was leached into the solution for further recycling, while the Fe component was retained in the residue as a FeC_2O_4 precipitate. Similarly, sodium peroxydisulfate ($Na_2S_2O_8$) was used to dissolve the SLICs; in this approach, the Fe component was transformed to a $FePO_4$ precipitate. Subsequently, the Li component was leached from the solution for recycling. In the third approach, a citric acid ($C_6H_8O_7$) solution was used to dissolve the SLICs, and subsequently NaOH solution was added to adjust the solution pH and precipitate the Fe_3O_4 species. Further details regarding the recycling and leaching processes are provided in Note S1.

FJH Upgrading of Fe-Enriched Residues from SLICs. The Fe-enriched residues obtained from the SLICs were upgraded by FJH treatment using a self-made system (Figure S1). Sawdust-derived biochar and Fe-enriched residues were uniformly mixed as precursors for further FJH upgrading (6 mmol Fe: 1 g biochar). Then, 0.1 g of the mixed precursors was loaded into a quartz tube and subjected to a direct current at an initial voltage of 250 V under negative pressure. After the appropriate treatment time (100 ms), the desired FJH-derived composites were obtained. The FJH-derived composites obtained following $H_2C_2O_4$, $Na_2S_2O_8$, and $C_6H_8O_7$ treatment were denoted as FeC_2O_4−FJH, $FePO_4$−FJH, and Fe_3O_4−FJH, respectively. Further details regarding the preparation of the pyrolysis-derived composites are provided in Note S2.

Characterization of FJH-Derived Fe Composites. The crystal structures of the FJH-derived composites were characterized by X-ray diffractometry (XRD) using Cu−Kα irradiation. The elemental species present in the prepared samples were determined by X-ray photoelectron spectroscopy (XPS). All XPS were calibrated using the standard C 1s peak at 284.8 eV. Raman spectroscopy (LabRam HR Evolution) was

https://doi.org/10.1021/acsestengg.4c00645
ACS EST Engg. XXXX, XXX, XXX−XXX

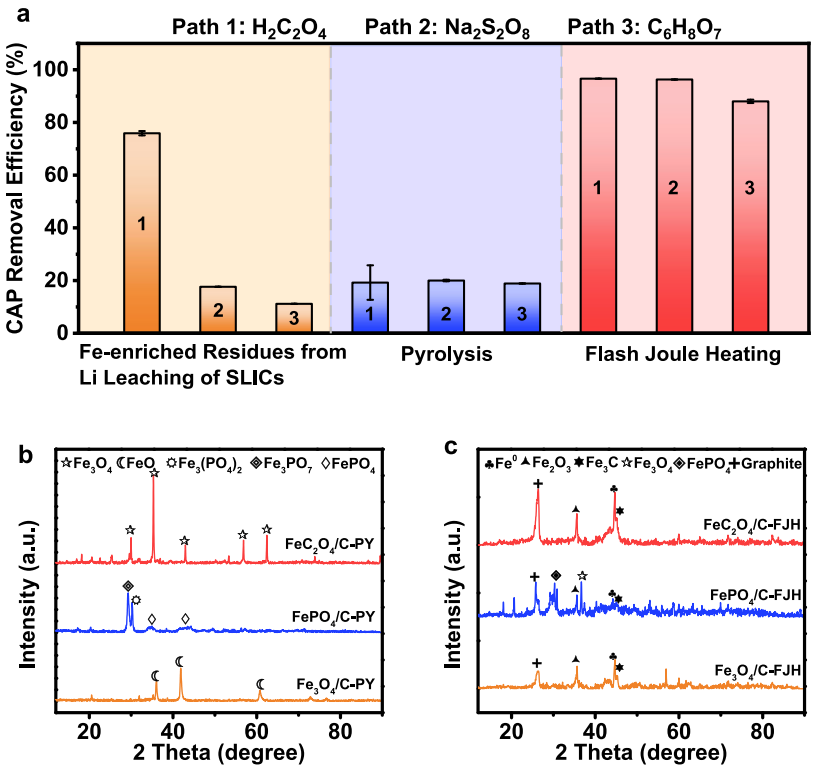

Figure 2. (a) CAP removal efficiency of Fe-enriched residues from Li leaching of SLICs within $H_2C_2O_4$, $Na_2S_2O_8$, and $C_6H_8O_7$ leaching pathways and their derived Fe materials fabricated by pyrolysis and FJH treatment [conducted at pH of 3, PDS concentration of 5 mol/L, and FJH-derived composites dosages of 1 mg/L]. (b) XRD spectra of pyrolysis-derived composites from Fe-enriched residues within three leaching paths. (c) XRD spectra of FJH-derived composites from Fe-enriched residues within three leaching paths.

performed to identify the degree of graphitization and the layers of the samples. X-ray absorption spectroscopy (XAS), including X-ray absorption near-edge structure (XANES) and extended X-ray absorption fine structure (EXAFS) analyses, was performed to characterize the FJH-derived composites at the Co K-edge (7709 eV). These analyses were carried out at the Singapore Synchrotron Light Source (SSLS) center using a pair of channel-cut Si(111) crystals in the monochromator. The Fe K-edge XANES data were recorded in transmission mode. Fe foil, FeO, Fe_3O_4, and Fe_2O_3 were used as the reference standards. The storage ring was operated at an energy of 2.5 GeV with an average electron current of <200 mA. The acquired EXAFS data were extracted and processed according to standard procedures using the ATHENA module implemented in the FEFIT software package.[2,3] The morphologies and elemental distributions of the samples were examined through transmission electron microscopy (TEM) combined with energy-dispersive X-ray spectroscopy (EDS).

CAP Degradation Assay to Measure FJH Upgrading Performance. The catalytic degradation of CAP was performed in a batch reactor. The FJH-derived composites (1 g/L) were mixed with sodium peroxydisulfate (PDS; 7 mM) to react with CAP solution (60 mg/L) at an initial pH of ~3, 150 rpm, and 25 °C in an oscillating chamber. As controls, the FJH-derived composites and PDS were independently added to CAP solutions (60 mg/L) and subjected to the same assay procedure. During each reaction, the CAP concentration was analyzed through high-performance liquid chromatography (HPLC) at a wavelength of 278 nm. The concentration of dissolved Fe^{2+} was determined according to the 1,10-phenanthroline method using an ultraviolet−visible (UV/vis) spectrophotometer at 510 nm.[23] Electron paramagnetic resonance (EPR) spectroscopy (Bruker EMXplus) was employed to identify the active radicals (i.e., $SO_4^{\bullet-}$ and $^{\bullet}OH$). Radical quenching experiments were also performed using *tert*-butanol (TBA) as a strong quencher of $^{\bullet}OH$, methanol as a strong quencher of $^{\bullet}OH$ and $SO_4^{\bullet-}$, and furfuryl alcohol (FFA) as a quencher of $^{\bullet}OH$, $SO_4^{\bullet-}$, and $^1O_2$. Further details regarding the quantitative analysis of the radicals are provided in Note S3. The performance of FJH-derived composites was further calculated by the catalytic degradation of bromate and florfenicol (FF). The FJH-derived composites (1 g/L) were mixed with sodium peroxydisulfate (PDS; 7 mM) to react with bromate and florfenicol (FF) solution (50 mg/L) at an initial pH of ~3, 150 rpm, and 25 °C in an oscillating chamber.

RESULTS AND DISCUSSION

Li Resource Leaching and FJH Upgrading of Fe-Enriched Residues. The pathways employed for Li leaching of SLICs and subsequent Fe-enriched residues are outlined in Figure 1a. During the $H_2C_2O_4$ leaching pathway, the Li leaching efficiency depended on the $H_2C_2O_4$ concentration in the leaching solution, in addition to the temperature, solid/liquid concentration, and leaching time (Figure S2). Following the optimization of the process conditions, >90% Li leaching efficiency was achieved for all three approaches at a leaching solution concentration of 0.3 mol/L, temperature of 80 °C, solid/liquid concentration of 60 g/L, and leaching time of 60 min (Figure 1b). These conditions also yielded a Fe retention efficiency of ~90.1% (Figure S2), indicating that the Fe-

https://doi.org/10.1021/acsestengg.4c00645
ACS EST Engg. XXXX, XXX, XXX−XXX

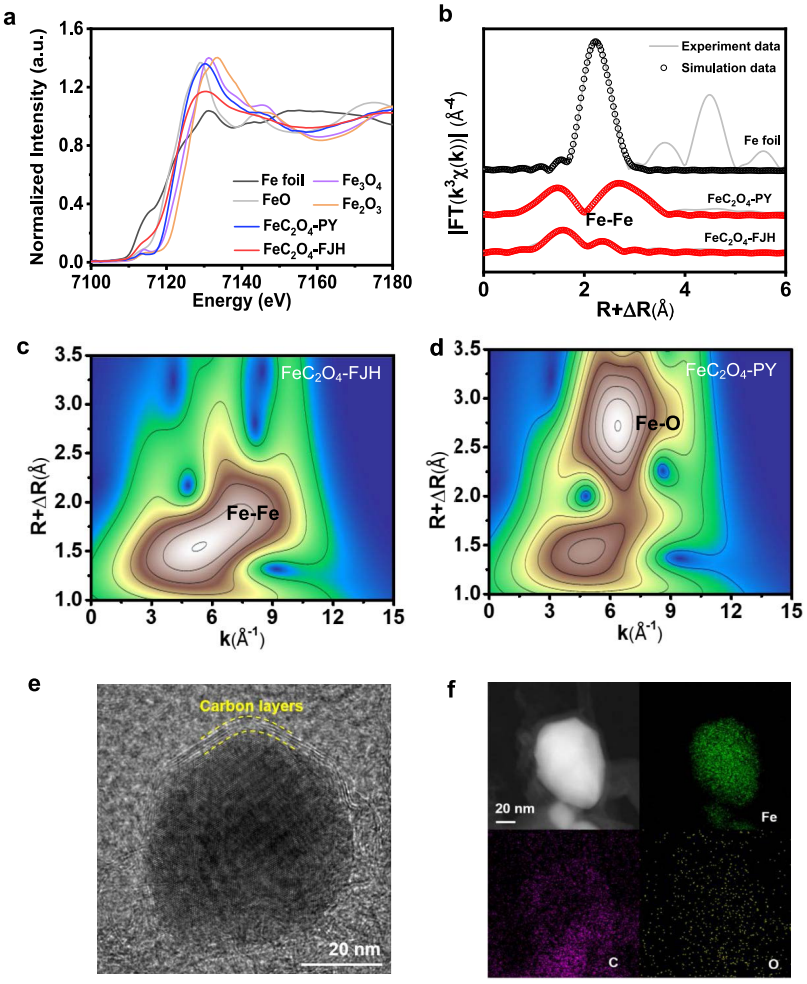

Figure 3. (a) Fe-XANES K-edge spectra of FeC_2O_4−FJH, FeC_2O_4−PY. (b) EXAFS spectra and fitting curves of Fe foil, FeC_2O_4−FJH, and FeC_2O_4−PY. Wavelet transform images of (c) FeC_2O_4−FJH and (d) FeC_2O_4−PY. (e) TEM image and (f) energy-dispersive spectroscopy (EDS) elemental mapping of C, Fe, and O elements distribution in FeC_2O_4−FJH.

enriched residues were effectively retained under all three pathways examined herein. As shown in the XRD patterns presented in Figure 1c, the crystal phases of the Fe-enriched residue obtained by $H_2C_2O_4$ leaching were mainly FeC_2O_4 and FeO(OH), while $FePO_4$ dominated following $Na_2S_2O_8$ leaching, and Fe_3O_4 was the most abundant component after $C_6H_8O_7$ leaching. These results suggest that the commonly employed SLICs leaching pathways produce a range of Fe species in the Fe-enriched residues.

To upgrade the Fe-enriched residues, FJH treatment was performed to fabricate Fe composites. Subsequently, the degradation of CAP within PDS activation by the Fe species was examined as a probe reaction to evaluate the performance of the Fe-enriched residues. As shown in Figure 2a, the FJH-derived composites exhibited significantly improved CAP removal efficiency compared to the raw Fe-enriched residue and pyrolysis-derived composite. Notably, the catalytic performance of the FJH-derived composites was found to be independent of the leaching pathways employed, which was confirmed by 96.6, 96.3, and 91.1% CAP removal efficiency by $H_2C_2O_4$, $Na_2S_2O_8$, and $C_6H_8O_7$ treatment, respectively (Figure 2a). More specifically, a CAP removal efficiency of ∼72.9% was achieved using the Fe-enriched residue obtained by $H_2C_2O_4$ leaching; this improvement was attributed to the activation of PDS by FeC_2O_4 (Figure 1c).[24] Moreover, in order to distinguish whether the removal of CAP is caused by adsorption or catalytic degradation of the composites, CAP adsorption of different FJH-derived composites was conducted (Figure S3). It was found that the absorption effect of the FJH-derived composites on CAP removal was weak, suggesting that removed CAP was mainly degraded by the FJH-derived composites. These results confirm that the FJH-derived composites exhibit a higher catalytic activation performance than those within traditional pyrolysis. It can therefore be inferred that the instantaneous ultrahigh temperature achievement and electrical stripping effect of the FJH treatment favored the formation of active Fe species for PDS activation, thereby promoting CAP degradation.

Structure Advantage of FJH-Derived Composites from Fe-Enriched Residues. To better understand the factors causing the improvement in the performance of the Fe-enriched residues upgraded by FJH treatment, the structures of the composites were examined in detail. According to the XRD patterns, iron oxides (Fe_3O_4 and FeO) were the main Fe species present in the pyrolysis-derived composites (FeC_2O_4−PY, $FePO_4$−PY, and Fe_3O_4−PY) owing to the low pyrolysis temperatures employed during treatment (Figure 2b). Notably, these iron oxides (Fe_3O_4 and FeO) cannot effectively activate PDS for CAP degradation.[25] In contrast, Fe^0, Fe_3C, and Fe_2O_3 were detected in the FJH-derived composites (FeC_2O_4−FJH,

https://doi.org/10.1021/acsestengg.4c00645
ACS EST Engg. XXXX, XXX, XXX−XXX

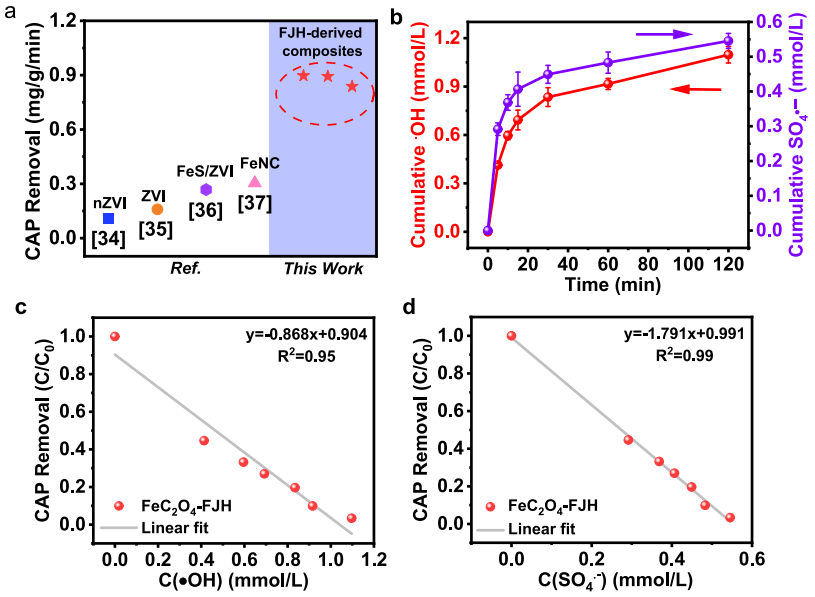

Figure 4. (a) Comparison of CAP degradation efficiency from similar advanced oxidation processes reacted systems, such as zerovalent iron and the composites prepared by conventional methods.[34−37] (b) Cumulative concentrations of ·OH and $SO_4^{\bullet-}$ produced from FeC_2O_4−FJH composite/PDS system. (c) Line fit of $^{\bullet}OH$ concentration and CAP removal with FeC_2O_4−FJH composite. (d) Line fit of $SO_4^{\bullet-}$ concentration and CAP removal with FeC_2O_4−FJH composite.

$FePO_4$−FJH, and Fe_3O_4−FJH; Figure 2c). The formation of Fe^0 was also confirmed by XPS of the FJH-derived composites (Figure S4). In addition, it should be noted that the abilities of Fe_3C and Fe_2O_3 to activate PDS were weaker than that of the Fe^0 component,[25] thereby implying that the high catalytic activity of the FJH-derived composites could be mainly attributed to the presence of Fe^0, which plays an important role in PDS activation.[26] Moreover, the instantaneous ultrahigh temperature achievement and electric stripping effect resulting from the ultrahigh current employed during FJH treatment (Figure S5) led to the efficient breakage of the Fe−O bonds to generate the active Fe^0 species.[27,28]

To further investigate the high reactivity of the FJH-derived composites, XANES and EXAFS analyses were performed on the FJH- and pyrolysis-derived composites produced by the $H_2C_2O_4$ leaching pathway. The XANES spectrum of FeC_2O_4−FJH presented in Figure 3a shows that the position of the rising edge was located between those of Fe foil and FeO, indicating that the average oxidation state of Fe in FeC_2O_4−FJH lied between Fe^0 and Fe^{2+}. Notably, the position of the rising edge in the XANES spectrum of FeC_2O_4−PY was located between those of Fe_3O_4 and Fe_2O_3, suggesting that the average oxidation state of Fe in FeC_2O_4−PY was between those of Fe^{3+} and Fe^{2+} (Figure 3a). These results indicate that Fe_3O_4 was the main Fe species in the pyrolysis-derived composites, whereas Fe^0 dominated in the FJH-derived composites, which was also confirmed by XRD analyses. Additionally, the Fourier transform k^3-weighted extended EXAFS results and fitting spectrum obtained for FeC_2O_4−FJH indicated the existence of Fe−Fe bonds with a distance of 2.87 Å, which is similar to the Fe−Fe bond distance in Fe foil (2.85 Å; Figure 3b and Table S1). Compared to those of the Fe_2O_3 and Fe_3O_4 standards, the O coordination number of Fe−O in the first shell of FeC_2O_4−FJH was reduced from 6 to 2, and the Fe coordination number of Fe−Fe in the second shell (bond distance = 2.87 Å) decreased to 3. These observations confirm that the partial cracking of the Fe−O bonds occurred at ultrahigh temperatures during FJH treatment to form low-coordinated Fe^0 component, thereby favoring electron transport.[29,30] In contrast, only Fe oxides were fit to the spectrum of FeC_2O_4−PY, indicating the difficulties associated with Fe−O bond breakage under the lower-temperature pyrolysis conditions employed herein (Figure S6). A comparison of the wavelet transform images of FeC_2O_4−FJH and FeC_2O_4−PY also implied breakage of the Fe−O bonds and the existence of low-coordinated Fe−Fe bonds in the FJH-derived composites (Figures 3c,d and S7). Overall, these data confirm that low-coordinated Fe^0 structures have positive effects on the catalytic performance of the FJH-derived composites.

Furthermore, the results of TEM combined with elemental mapping showed that Fe was uniformly dispersed as nanoparticles in the FeC_2O_4−FJH sample (Figure 3e,f). This was mainly attributed to the instantaneous ultrahigh temperature achievement and electric stripping effect of FJH treatment, which prevents metal agglomeration and promotes nanoparticle formation during ultrafast cooling.[31,32] In addition, FJH treatment was found to enhance the graphitization of the carbon substrate (Figure S8), which led to faster electron transfer for higher CAP degradation efficiency.[33] In contrast, the carbon substrate of the pyrolysis-derived composite exhibited a lower graphitization degree owing to the low temperature and absence of the electric stripping effect (Figure S9). Thus, it can be inferred that the low-coordinated Fe^0 nanoparticles in FJH-derived composites may activate PDS to a greater extent than pyrolysis-derived composites, thereby enhancing CAP degradation.

Mechanism of CAP Degradation by FJH-Derived Composites. The mechanism of CAP degradation by PDS in the presence of the FJH-derived composites was subsequently evaluated. As presented in Figure S10, a removal efficiency of ∼96.6% was obtained for the FeC_2O_4−FJH and $FePO_4$−FJH specimens, while a similar removal efficiency of

https://doi.org/10.1021/acsestengg.4c00645
ACS EST Engg. XXXX, XXX, XXX−XXX

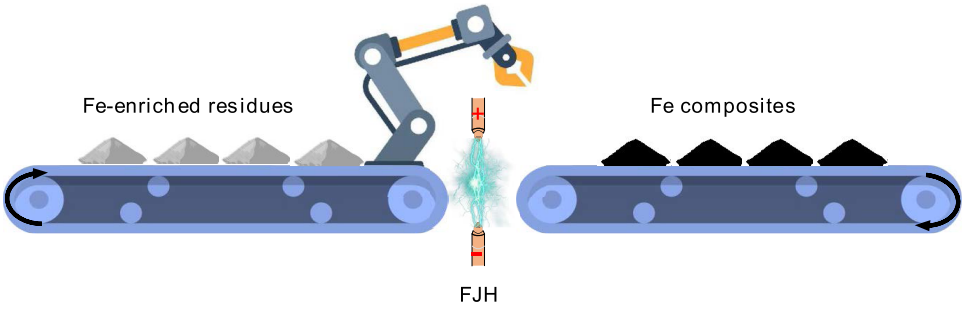

Figure 5. Continuous device for large-scale fabrication of the FJH-derived composites via automated production.

~91.1% was achieved for the Fe_3O_4−FJH sample. As expected, the FJH-derived composites exhibited higher CAP removal efficiency than the Fe-based composites prepared by conventional methods[34−37] (Figure 4a), thereby indicating that FJH treatment is a promising method for upgrading Fe-enriched residues.[34−37]

EPR spectroscopy was performed to identify the surface-bound radicals present in the reaction system,[38] with only $SO_4^{\bullet-}$ and $^{\bullet}OH$ being detected (Figure S11). A series of quenching experiments were also conducted to identify the contribution of reactive oxygen species (ROS) to the CAP degradation process and explore the reason for the enhanced activities demonstrated by the FJH-derived composites.[39] As shown in Figure S12, surface-bound $SO_4^{\bullet-}$ and $^{\bullet}OH$ species were regarded as the main ROS present during the CAP degradation process catalyzed by the FJH-derived composites. In addition, the CAP degradation efficiency was found to be positively correlated with the $SO_4^{\bullet-}$ and $^{\bullet}OH$ concentrations (Figure 4c,d),[40,41] further confirming the active role of these species during CAP degradation. Furthermore, the $^{\bullet}OH$ and Fe^{2+} concentrations were found to be positively correlated with one another (Figure S13), implying that Fe^{2+} could be produced by oxidation of the low-coordinated Fe^0 species, resulting in CAP degradation.[25] Thus, the low-coordinated Fe^0 present in these composites plays a key role in the degradation of CAP via PDS activation.

Finally, a series of realistic parameters were used to investigate the practicability of the FJH-derived composites. As shown in Figure S14, FeC_2O_4−FJH exhibits satisfactory performance over a wide range of pH values, catalyst dosages, and PDS concentrations. In addition, the FJH-derived composites exhibited high removal efficiency for the direct reduction of bromate and fluorfenicol due to the presence of low-coordinated Fe^0 components (Figure S15). Consequently, FJH treatment was identified as a promising method for the treatment of SLICs to provide useful active compounds.

Environmental Implications. FJH treatment has emerged as a promising method for upgrading Fe-enriched residues from Li leaching of SLICs. The instantaneous FJH process induced Fe-enriched residues into composites with active low-coordinated Fe^0 species, thereby overcoming the limitations of the conventional pyrolysis method. Thus, the resulting FJH-derived composites promoted PDS activation to produce ROS and enhanced the removal efficiency of CAP. Furthermore, the energy consumption of conventional pyrolysis was 34 times higher than that of FJH treatment, which was presented in a previous study.[21] Notably, a continuous device for the automated production of the FJH-derived composites was developed (Figure 5), including transmission, mechanical transfer, and reaction functions, wherein the robot arm continuously transferred the raw material from the loading area to the reaction area. This unit can be further scaled up to achieve factory-scale production efficiency for the large-scale and low-energy production of composites for industrialization.

■ ASSOCIATED CONTENT

Supporting Information

The Supporting Information is available free of charge at https://pubs.acs.org/doi/10.1021/acsestengg.4c00645.

Details of Li leaching for SLICs; FJH upgrading of Fe-enriched residues from SLICs; quantitative analysis of hydroxyl radical; schematic of the homemade FJH equipment; effects on Li leaching efficiency; adsorption effect of different FJH-derived composites on chloramphenicol (CAP) degradation; Fe 2p XPS spectra; real-time current and voltage of the FJH treatment; EXAFS fitting curves; wavelet transform images; Raman spectra; CAP removal of FJH-derived composites; EPR spectra of $^{\bullet}OH$ and $SO_4^{\bullet-}$; contributions of radicals on CAP removal; transformation of Fe species; effects on CAP removal; bromate and florfenicol removal; and EXAFS fitting parameters (PDF)

■ AUTHOR INFORMATION

Corresponding Author

Xiangdong Zhu − *Department of Environmental Science and Engineering, Fudan University, Shanghai 200438, China; State Key Laboratory of Soil and Sustainable Agriculture, Institute of Soil Science, Chinese Academy of Sciences, Nanjing 210008, China;* orcid.org/0000-0002-8536-7690; Email: zxdjewett@fudan.edu.cn, xdzhu@issas.ac.cn

Authors

Hua Shang − *Biofuels Institute, School of the Environment and Safety Engineering, Jiangsu University, Zhenjiang 212013, China;* orcid.org/0000-0003-4278-4512

Wenting Yang − *Jiangsu Shangding New Energy Technology Co., Ltd, Suzhou 215000, China*

Zhelin He − *Department of Environmental Science and Engineering, Fudan University, Shanghai 200438, China*

Jiewen Luo − *Guangdong Key Laboratory of Integrated Agro-environmental Pollution Control and Management, Institute of Eco-environmental and Soil Sciences, Guangdong Academy of Sciences, Guangzhou 510650, China*

Fengbo Yu − *Department of Environmental Science and Engineering, Fudan University, Shanghai 200438, China; State Key Laboratory of Soil and Sustainable Agriculture, Institute of Soil Science, Chinese Academy of Sciences, Nanjing 210008, China*

https://doi.org/10.1021/acsestengg.4c00645
ACS EST Engg. XXXX, XXX, XXX−XXX

Chao Jia − *Department of Environmental Science and Engineering, Fudan University, Shanghai 200438, China; State Key Laboratory of Soil and Sustainable Agriculture, Institute of Soil Science, Chinese Academy of Sciences, Nanjing 210008, China*

Complete contact information is available at: https://pubs.acs.org/10.1021/acsestengg.4c00645

Author Contributions

H.S.: conceptualization; methodology; investigation; formal analysis; data curation; visualization; and writing—original draft; W.Y.: resource; supervision; and investigation; Z.H.: investigation and data curation; J.L.: visualization; F.Y. and C.J.: investigation; X.Z.: conceptualization; methodology; formal analysis; data curation; supervision; funding acquisition; and writing—review and editing. CRediT: **Hua Shang** conceptualization, data curation, formal analysis, investigation, methodology, visualization, writing - original draft; **Wenting Yang** investigation, resources, supervision; **Zhelin He** data curation, investigation; **Jiewen Luo** visualization; **Fengbo Yu** investigation; **Chao Jia** investigation; **Xiangdong Zhu** conceptualization, data curation, formal analysis, funding acquisition, methodology, supervision, writing - review & editing.

Notes

The authors declare no competing financial interest.

■ ACKNOWLEDGMENTS

This work was supported by the National Natural Science Foundation of China (No. 22276040).

■ REFERENCES

(1) Harper, G.; Sommerville, R.; Kendrick, E.; Driscoll, L.; Slater, P.; Stolkin, R.; Walton, A.; Christensen, P.; Heidrich, O.; Lambert, S.; Abbott, A.; Ryder, K.; Gaines, L.; Anderson, P. Recycling lithium-ion batteries from electric vehicles. *Nature* **2019**, *575*, 75−86.

(2) Sun, X.; Ouyang, M.; Hao, H. Surging lithium price will not impede the electric vehicle boom. *Joule* **2022**, *6*, 1738−1742.

(3) Sun, Q.; Li, X.; Zhang, H.; Song, D.; Shi, X.; Song, J.; Li, C.; Zhang, L. Resynthesizing $LiFePO_4$/C materials from the recycled cathode via a green full-solid route. *J. Alloys Compd.* **2020**, *818*, No. 153292.

(4) Zhou, J.; Xing, C.; Huang, J.; Zhang, Y.; Li, G.; Chen, L.; Tao, S.; Yang, Z.; Wang, G.; Fei, L. Direct upcycling of leached $FePO_4$ from spent lithium-ion batteries toward gradient—doped $LiMnxFe_1-xPO_4$ cathode material. *Adv. Energy Mater.* **2023**, *14*, No. 2302761.

(5) Lei, S.; Sun, W.; Yang, Y. Comprehensive technology for recycling and regenerating materials from spent lithium iron phosphate battery. *Environ. Sci. Technol.* **2024**, *58*, 3609−3628.

(6) Zhang, L.; Zhang, Y.; Xu, Z.; Zhu, P. The foreseeable future of spent lithium-ion batteries: advanced upcycling for toxic electrolyte, cathode, and anode from environmental and technological perspectives. *Environ. Sci. Technol.* **2023**, *57*, 13270−13291.

(7) Fan, E.; Li, L.; Wang, Z.; Lin, J.; Huang, Y.; Yao, Y.; Chen, R.; Wu, F. Sustainable recycling technology for Li-ion batteries and beyond: Challenges and future prospects. *Chem. Rev.* **2020**, *120*, 7020−7063.

(8) Zhou, M.; Li, B.; Li, J.; Xu, Z. Pyrometallurgical technology in the recycling of a spent lithium ion battery: Evolution and the challenge. *ACS ES&T Eng.* **2021**, *1*, 1369−1382.

(9) Mrozik, W.; Rajaeifar, M. A.; Heidrich, O.; Christensen, P. Environmental impacts, pollution sources and pathways of spent lithium-ion batteries. *Energy Environ. Sci.* **2021**, *14*, 6099−6121.

(10) Liu, J.; Peng, C.; Shi, X. Preparation, characterization, and applications of Fe-based catalysts in advanced oxidation processes for organics removal: A review. *Environ. Pollut.* **2022**, *293*, No. 118565.

(11) Jie, Y.; Yang, S.; Li, Y.; Hu, F.; Zhao, D.; Chang, D.; Lai, Y.; Chen, Y. Waste organic compounds thermal treatment and valuable cathode materials recovery from spent $LiFePO_4$ batteries by vacuum pyrolysis. *ACS Sustainable Chem. Eng.* **2020**, *8*, 19084−19095.

(12) Deng, B.; Luong, D. X.; Wang, Z.; Kittrell, C.; McHugh, E. A.; Tour, J. M. Urban mining by flash Joule heating. *Nat. Commun.* **2021**, *12*, No. 5794.

(13) Qiao, J.; Jiao, W.; Liu, Y. Degradation of nitrobenzene-containing wastewater by sequential nanoscale zero valent iron-persulfate process. *Green Energy Environ.* **2021**, *6*, 910−919.

(14) Chong, Y.; Ge, C.; Fang, G.; Wu, R.; Zhang, H.; Chai, Z.; Chen, C.; Yin, J. J. Light-enhanced antibacterial activity of graphene oxide, mainly via accelerated electron transfer. *Environ. Sci. Technol.* **2017**, *51*, 10154−10161.

(15) Huang, P.; Zhang, P.; Wang, C.; Du, X.; Jia, H.; Sun, H. P-doped biochar regulates nZVI nanocracks formation for superefficient persulfate activation. *J. Hazard. Mater.* **2023**, *450*, No. 130999.

(16) Wang, K.; Liu, X.; Tang, J.; Wang, L.; Sun, H. Ball milled Fe^0@FeS hybrids coupled with peroxydisulfate for Cr(VI) and phenol removal: Novel surface reduction and activation mechanisms. *Sci. Total Environ.* **2020**, *739*, No. 139748.

(17) Yu, F.; Jia, C.; Wu, X.; Sun, L.; Shi, Z.; Teng, T.; Lin, L.; He, Z.; Gao, J.; Zhang, S.; Wang, L.; Wang, S.; Zhu, X. Rapid self-heating synthesis of Fe-based nanomaterial catalyst for advanced oxidation. *Nat. Commun.* **2023**, *14*, No. 4975.

(18) Jia, C.; Sun, L.; Wu, X.; Yu, F.; Lin, L.; He, Z.; Gao, J.; Zhang, S.; Zhu, X. Joule heating induced reductive iron−magnesium bimetallic banocomposite for eminent heavy metal removal. *ACS ES&T Eng.* **2024**, *4*, 938−946.

(19) Deng, B.; Wang, Z.; Chen, W.; Li, J. T.; Luong, D. X.; Carter, R. A.; Gao, G.; Yakobson, B. I.; Zhao, Y.; Tour, J. M. Phase controlled synthesis of transition metal carbide nanocrystals by ultrafast flash Joule heating. *Nat. Commun.* **2022**, *13*, No. 262.

(20) Dong, Q.; Yao, Y.; Cheng, S.; Alexopoulos, K.; Gao, J.; Srinivas, S.; Wang, Y.; Pei, Y.; Zheng, C.; Brozena, A. H.; Zhao, H.; Wang, X.; Toraman, H. E.; Yang, B.; Kevrekidis, I. G.; Ju, Y.; Vlachos, D. G.; Liu, D.; Hu, L. Programmable heating and quenching for efficient thermochemical synthesis. *Nature* **2022**, *605*, 470−476.

(21) Yu, F.; Jia, C.; Wu, X.; Sun, L.; Shi, Z.; Teng, T.; Lin, L.; He, Z.; Gao, J.; Zhang, S.; et al. Rapid self-heating synthesis of Fe-based nanomaterial catalyst for advanced oxidation. *Nat. Commun.* **2023**, *14*, 4975.

(22) Luong, D. X.; Bets, K. V.; Algozeeb, W. A.; Stanford, M. G.; Kittrell, C.; Chen, W.; Salvatierra, R. V.; Ren, M.; McHugh, E. A.; Advincula, P. A.; et al. Gram-scale bottom-up flash graphene synthesis. *Nature* **2020**, *577*, 647−651.

(23) Kim, C.; Ahn, J.-Y.; Kim, T. Y.; Shin, W. S.; Hwang, I. Activation of persulfate by nanosized zero-valent iron (NZVI): mechanisms and transformation products of NZVI. *Environ. Sci. Technol.* **2018**, *52*, 3625−3633.

(24) Fu, Q.; Mu, Y.; Yang, L.; Mei, Y.; Wu, M.; Zou, J.-P.; Dionysiou, D. D.; Luo, S. Hydroxyl radical streaming from molecular oxygen activation by β-$FeC_2O_4 \cdot 2H_2O$ for efficiently degrading Microcystin-LR. *Appl. Catal., B* **2023**, *321*, No. 121970.

(25) Wu, Y.; Chen, X.; Han, Y.; Yue, D.; Cao, X.; Zhao, Y.; Qian, X. Highly efficient utilization of nano-Fe(0) embedded in mesoporous carbon for activation of peroxydisulfate. *Environ. Sci. Technol.* **2019**, *53*, 9081−9090.

(26) Ma, D.; Yang, Y.; Liu, B.; Xie, G.; Chen, C.; Ren, N.; Xing, D. Zero-valent iron and biochar composite with high specific surface area via K_2FeO_4 fabrication enhances sulfadiazine removal by persulfate activation. *Chem. Eng. J.* **2021**, *408*, No. 127992.

(27) Zhu, X.; Lin, L.; Pang, M.; Jia, C.; Xia, L.; Shi, G.; Zhang, S.; Lu, Y.; Sun, L.; Yu, F.; Gao, J.; He, Z.; Wu, X.; Li, A.; Wang, L.; Wang, M.; Cao, K.; Fu, W.; Chen, H.; Li, G.; Zhang, J.; Wang, Y.; Yang, Y.;

Zhu, Y. G. Continuous and low-carbon production of biomass flash graphene. *Nat. Commun.* **2024**, *15*, No. 3218.
(28) Yao, Y.; Huang, Z.; Xie, P.; Lacey, S. D.; Jacob, R. J.; Xie, H.; Chen, F.; Nie, A.; Pu, T.; Rehwoldt, M.; Yu, D.; Zachariah, M. R.; Wang, C.; Shahbazian-Yassar, R.; Li, J.; Hu, L. Carbothermal shock synthesis of high-entropy-alloy nanoparticles. *Science* **2018**, *359*, 1489−1494.
(29) Sun, L.; Wu, X.; Jiao, Y.; Jia, C.; Teng, T.; Lin, L.; Yu, F.; He, Z.; Gao, J.; Yan, S.; Shi, G.; Ren, Z. J.; Yang, J.; Zhang, S.; Zhu, X. Millisecond self-heating and quenching synthesis of Fe/carbon nanocomposite for superior reductive remediation. *Appl. Catal., B* **2024**, *342*, No. 123361.
(30) Liu, Y.; Cheng, J.; Deng, L. Three-coordinate formal Cobalt(0), Iron(0), and Manganese(0) complexes with persistent carbene and alkene ligation. *Acc. Chem. Res.* **2020**, *53*, 244−254.
(31) Wu, X.; Jiao, Y.; Jia, C.; Sun, L.; Yu, F.; Lin, L.; Gao, J.; Teng, T.; He, Z.; Li, A.; Zhang, S.; Yang, J.; Wang, S.; Zhu, X. Joule heating-induced active Mg^0 into nano-Mg composites for boosted oxidation and antiviral performance. *ACS ES&T Eng.* **2024**, *4*, 1302−1311.
(32) Xie, H.; Liu, Y.; Li, N.; Li, B.; Kline, D. J.; Yao, Y.; Zachariah, M. R.; Wang, G.; Su, D.; Wang, C.; Hu, L. High-temperature-pulse synthesis of ultrathin-graphene-coated metal nanoparticles. *Nano Energy* **2021**, *80*, No. 105536.
(33) Zhang, C.; Wang, D.; Liu, Q.; Tang, J. Ligand-citric acid enhanced in-situ ROS generation by GBC@nZVI to promote the aerobic degradation of adsorbed 2,4-dichlorophenol. *Chem. Eng. J.* **2023**, *477*, No. 147126.
(34) Zhang, T.; Yang, Y.; Gao, J.; Li, X.; Yu, H.; Wang, N.; Du, P.; Yu, R.; Li, H.; Fan, X.; Zhou, Z. Synergistic degradation of chloramphenicol by ultrasound-enhanced nanoscale zero-valent iron/persulfate treatment. *Sep. Purif. Technol.* **2020**, *240*, No. 116575.
(35) Tan, C.; Dong, Y.; Fu, D.; Gao, N.; Ma, J.; Liu, X. Chloramphenicol removal by zero valent iron activated peroxymonosulfate system: Kinetics and mechanism of radical generation. *Chem. Eng. J.* **2018**, *334*, 1006−1015.
(36) Dai, Y.; Du, W.; Jiang, C.; Wu, W.; Dong, Y.; Duan, L.; Sun, S.; Zhang, B.; Zhao, S. Enhanced reductive degradation of chloramphenicol by sulfidated microscale zero-valent iron: Sulfur-induced mechanism, competitive kinetics, and new transformation pathway. *Water Res.* **2023**, *233*, No. 119743.
(37) Wu, H.; Gao, Y.; Xu, X.; Li, X.; Cui, J.; Lin, A. Efficient activation of peroxydisulfate by FeNC for chloramphenicol degradation: Performance and mechanisms. *J. Cleaner Prod.* **2022**, *380*, No. 134981.
(38) Zhuo, S. N.; Ren, H. Y.; Cao, G. L.; Xie, G. J.; Xing, D. F.; Ren, N. Q.; Liu, B. F. Highly efficient activation of persulfate by encapsulated nano-Fe0 biochar for acetaminophen degradation: Rich electron environment and dominant effect of superoxide radical. *Chem. Eng. J.* **2022**, *440*, No. 135947.
(39) Liang, J.; Li, K.; Shi, F.; Li, J.; Gu, Jn.; Xue, Y.; Bao, C.; Guo, M.; Jia, J.; Fan, M.; Sun, T. Constructing high-performance cobalt-based environmental catalysts from spent lithium-ion batteries: unveiling overlooked roles of copper and aluminum from current collectors. *Angew. Chem., Int. Ed.* **2024**, *63*, No. e202407870.
(40) Wang, D.; Huang, D.; Wu, S.; Fang, G.; Zhu, F.; Chen, N.; Liu, S.; Zhu, C.; Zhou, D. Pyrogenic carbon initiated the generation of hydroxyl radicals from the oxidation of sulfide. *Environ. Sci. Technol.* **2021**, *55*, 6001−6011.
(41) Oh, W. D.; Dong, Z.; Ronn, G.; Lim, T. T. Surface−active bismuth ferrite as superior peroxymonosulfate activator for aqueous sulfamethoxazole removal: Performance, mechanism and quantification of sulfate radical. *J. Hazard. Mater.* **2017**, *325*, 71−81.

https://doi.org/10.1021/acsestengg.4c00645
ACS EST Engg. XXXX, XXX, XXX−XXX